POLYOXOMETALATES

Open Access
RESEARCH ARTICLE

Polyoxometalates as a precursor in one-pot synthesis of MoS_2-V_2O_5@CC for electrocatalytic hydrogen evolution

Sizhan Shu[1], Xiao Feng[1], Jun Sun[1], Qiaoshun Chen[1], Shengyang Ou[1], Shuxin Zhang[1], Yuhan Li[1], and Pingfan Wu[1,2] ✉

[1] *Institute of POM-based Materials, Hubei provincial Key Laboratory of Green Materials for Light Industry, Hubei University of Technology, Wuhan 430068, China*
[2] *Hubei Longzhong Lab, Xiangyang 441000, China*

Cite This: *Polyoxometalates*, **2026**, *5*, 9140125

Read Online

ABSTRACT: Polyoxometalates (POMs) are ideal preassembled platforms for constructing transition metal catalysts because they are rich in oxygen and transition metal elements. In contrast to traditional methods for preparing V_2O_5/MoS_2 composite catalysts, the method proposed in this study leverages the selective preference of vanadium for oxygen vs. sulfur. A MoS_2-based electrocatalyst composited with a small amount of V_2O_5 was constructed *in situ* on a carbon cloth via a one-pot hydrothermal method using a Lindqvist-type POM, i.e., $(C_{16}H_{36}N)_2Mo_3V_3O_{16}(OCH_2)_3CCH_2CH_3$ (Mo_3V_3), as a precursor. This catalyst was used for efficient electrocatalytic hydrogen evolution reaction. The experimental results reveal that the introduction of a small amount of V_2O_5 considerably increases the electrochemically active surface area of the catalyst, effectively enhancing the catalytic performance of the material. This study provides a new design strategy and synthetic pathway for precise construction of high-performance composite electrocatalysts based on POM precursors.

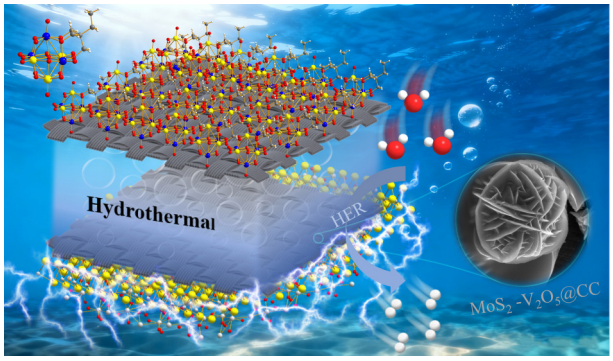

KEYWORDS: polyoxometalates, MoS_2, V_2O_5, heterojunctions, hydrogen evolution reaction

1 Introduction

The development of highly efficient and stable electrocatalysts is crucial for the advancement of water electrolysis technology for hydrogen production [1–4]. Recently, two-dimensional layered MoS_2 has attracted widespread attention owing to its intrinsic activity for hydrogen evolution reaction (HER), which is close to that of the precious metal platinum [5, 6]. However, the large-scale practical application of MoS_2 is restricted by its low intrinsic electrical conductivity and limited number of active sites [7, 8]. To overcome these limitations, researchers have composited MoS_2 with other functional materials to synergistically enhance its performance.

Vanadium pentoxide (V_2O_5) is an attractive modifier owing to its layered structure, making it highly compatible with MoS_2, which enables them to form stable heterojunctions [9, 10]. Theoretical and experimental studies suggest that these V_2O_5/MoS_2 interfaces can facilitate charge transfer and expose additional active sites, compensating for the shortcomings of pure MoS_2 [11–14]. However, the full realization of this synergistic potential critically depends on the synthesis method of the composite.

Current synthesis strategies of V_2O_5/MoS_2 composites fall into two main categories: physical mixing and hydrothermal synthesis, and each category has inherent limitations. Physical mixing requires the pre-synthesis of V_2O_5 and MoS_2. These components are then mixed using ultrasonication and subjected to a subsequent high-temperature hydrothermal treatment to form a MoS_2-V_2O_5 nanocomposite [15–17]. Although this approach offers several advantages, such as operational control and tunable ratios, it also has drawbacks. For example, the preparation cycle is long and the steps are cumbersome. More importantly, it often fails to achieve uniform component dispersion and good interfacial contact at the nanoscale. This results in a weak heterojunction effect and low efficiency of interfacial charge separation.

Haldar et al. [18] first used hydrothermal synthesis to prepare MoS_2-V_2O_5 nanocomposites by synthesizing MoS_2 via a hydrothermal treatment followed by a secondary hydrothermal reaction with $VOSO_4$. Although multistep hydrothermal approaches partially improve interfacial contact, their procedures remain complex. In comparison, Yu et al. [19]. employed a one-step hydrothermal method that involves dissolving ammonium vanadate, sodium molybdate, and thioacetamide in deionized water to prepare V_2O_5@MoS_2 composite material containing a small

Received: November 27, 2025; **Revised:** January 21, 2026
Accepted: February 19, 2026

✉Address correspondence to pingfanwu-111@163.com

https://doi.org/10.26599/POM.2026.9140125

amount of MoS_2, which was achieved by controlling the Mo/S ratio. However, the chemical state of vanadium is highly sensitive to synthesis conditions, especially to the type and dosage of the sulfur source. For instance, excessive sulfur may drive uncontrollable conversion of vanadium into VS_2 [20] or induce the hydrolysis of vanadium oxides. Therefore, exploring a facile and effective synthetic route for the rational design of active sites is critical to the fabrication of high‐efficiency MoS_2-V_2O_5 composite catalysts.

Polyoxometalates (POMs) comprise transition metal atoms (e.g., Mo, V, and W) linked by oxygen bridges. Their well-defined, "preassembled" nanocluster structures provide an ideal molecular platform for the design and fabrication of highly efficient catalytic materials [21, 22]. Unlike traditional precursors, POMs achieve uniform mixing and preorganization of metal elements at the atomic level. POMs can serve as perfect "single-source precursors" because they are directly converted into the target catalyst through one-step reactions [23–25]. Furthermore, POMs can be a rich oxygen source. Under pyrolysis or hydrothermal conditions, they can be transformed *in situ* into the target metal oxides or sulfides while maintaining a spatially uniform distribution of elements. Thus, they effectively overcome common issues in traditional methods such as phase separation and agglomeration [26]. Therefore, using POMs as precursors offers a promising technical pathway to address the challenge of precise compositing of V_2O_5/MoS_2 composites and to achieve control of the components at the atomic scale.

Herein, we constructed a Lindqvist-type POM, $(C_{16}H_{36}N)_2Mo_3V_3O_{16}(OCH_2)_3CCH_2CH_3$ (Mo_3V_3), with a precise Mo/V ratio of 1:1 via anchoring with a trimethylolpropane (Tris-Et) ligand. Accordingly, we developed a novel and efficient one-pot hydrothermal strategy to grow MoS_2-V_2O_5 composite nanomaterials *in situ* on a conductive carbon cloth (CC) substrate (MoS_2-V_2O_5@CC). The core advantage of this strategy lies in leveraging the distinct chemical behaviors of the precursor elements during the sulfurization process, enabling precise control over the product. In particular, one portion of the vanadium selectively forms V_2O_5 nanoparticles, and the other part is doped into the MoS_2 lattice. This achieves uniform *in situ* compositing of V_2O_5 within the MoS_2 matrix. Electrochemical studies show that the introduction of V_2O_5 effectively improves the charge transfer efficiency and increases the number of intrinsic active sites in the catalyst. The optimized MoS_2-V_2O_5@CC exhibits an overpotential of 244 mV at a current density of 100 mA·cm^{-2}. This performance is considerably superior to that of pure MoS_2@CC (312 mV) and V_2O_5@CC (808 mV). This study provides a simple, efficient, and controllable new pathway for preparing high-performance MoS_2-based HER catalysts and deepens our understanding of using POM precursors to construct complex metal sulfide/oxide heterojunctions. Moreover, it offers new methodological insights for designing related electrocatalysts.

2 Experimental section

2.1 Chemicals and instruments

$(TBA)_4[Mo_8O_{26}]$ (Mo_8, TBA = tetrabutylammonium) and $(TBA)_3[H_3V_{10}O_{28}]$ (V_{10}) were prepared according to the reported method [27]. Acetonitrile was dried over calcium hydride (CaH_2) and distilled before use. All other chemicals were purchased from commercial sources. They were of analytical grade and were used without further purification.

2.2 Synthesis of Mo_3V_3

In the synthesis [27], V_{10} (0.189 mmol), Mo_8 (0.189 mmol), and trimethylolpropane (0.615 mmol) were dissolved in acetonitrile (10 mL). The mixture was stirred using a constant-temperature magnetic stirrer until completely dissolved. The solution was then transferred into a microwave reactor. The reactor was sealed and placed in the microwave reaction system. The reaction temperature was set to 110 °C, with an upper limit of 130 °C. The reaction time was divided into ramp time (10 min) and hold time (15 min). The microwave power was capped at 1000 W. After the reaction, a reddish-brown solution was obtained. This solution was filtered into diethyl ether (60 mL) under rapid stirring, yielding a brown precipitate. Vapor diffusion was performed on this precipitate using acetonitrile as a good solvent and diethyl ether as a poor solvent, resulting in the orange block-shaped crystals of the target product (Mo_3V_3, yield based on V = 55%).

2.3 Catalyst synthesis

Synthesis of MoS_2-V_2O_5@CC: Mo_3V_3 (0.30 mmol) and thiourea (7.50 mmol) were dissolved in deionized water (30 mL). A piece of pretreated CC (3 cm × 2 cm) was added. The mixture was sonicated for 30 min. It was then subjected to a hydrothermal reaction at 180 °C for 24 h. After the reaction, the CC was collected by filtration. Next, it was washed with water and ethanol and then dried at room temperature (20–30 °C) for half a day. The dried CC was placed in a H_2/Ar gas mixture. The temperature was raised to 400 °C at a rate of 5 °C·min^{-1}, followed by calcination at this temperature for 2 h. The final measured loading amount was 2.2 mg·cm^{-2}.

Synthesis of MoS_2@CC: MoS_2@CC was prepared using the same method as MoS_2-V_2O_5@CC, except that Mo_3V_3 was replaced by Mo_8. The final measured loading amount was 4.1 mg·cm^{-2}.

Synthesis of V_2O_5@CC: V_2O_5@CC was prepared using the same method as MoS_2-V_2O_5@CC, except that Mo_3V_3 was replaced by V_{10}. The final measured loading amount was 0.5 mg·cm^{-2}.

2.4 Electrochemical measurements

All electrochemical tests were performed at room temperature using a CHI760E electrochemical workstation. Before testing, N_2 was bubbled through the electrolyte solution for 30 min to remove dissolved oxygen. A standard three-electrode system was used to evaluate the electrocatalytic activity. Hg/HgO (in KOH, 1 M), a platinum sheet, and the modified CC (tested area = 1 cm × 1 cm) served as the reference, counter, and working electrodes, respectively. Linear sweep voltammetry (LSV) measurements were performed in a KOH solution (1.0 M) at a scan rate of 2 mV·s^{-1}. The onset overpotential was determined from the linear region of the Tafel plot. The exchange current density was obtained by extrapolating the Tafel plot. Cyclic voltammetry (CV) tests were conducted at 0.1–0.2 V (vs. reversible hydrogen electrode, RHE) and scan rates of 5, 8, 11, 14, 17, 20, 23, and 26 mV·s^{-1}. Electrochemical impedance spectroscopy (EIS) measurements were performed over a frequency range of 10^{-2}–10^6 Hz, with an amplitude of 5 mV. All potentials were converted to the RHE scale using the following equation: $E_{RHE} = E_{Hg/HgO} + 0.098\ V + 0.059 \times pH$ (in KOH, 1 M). All data were adjusted for 90% *iR* compensation.

3 Results and discussion

As shown in Scheme 1, Mo_3V_3 was used as the Mo and V sources,

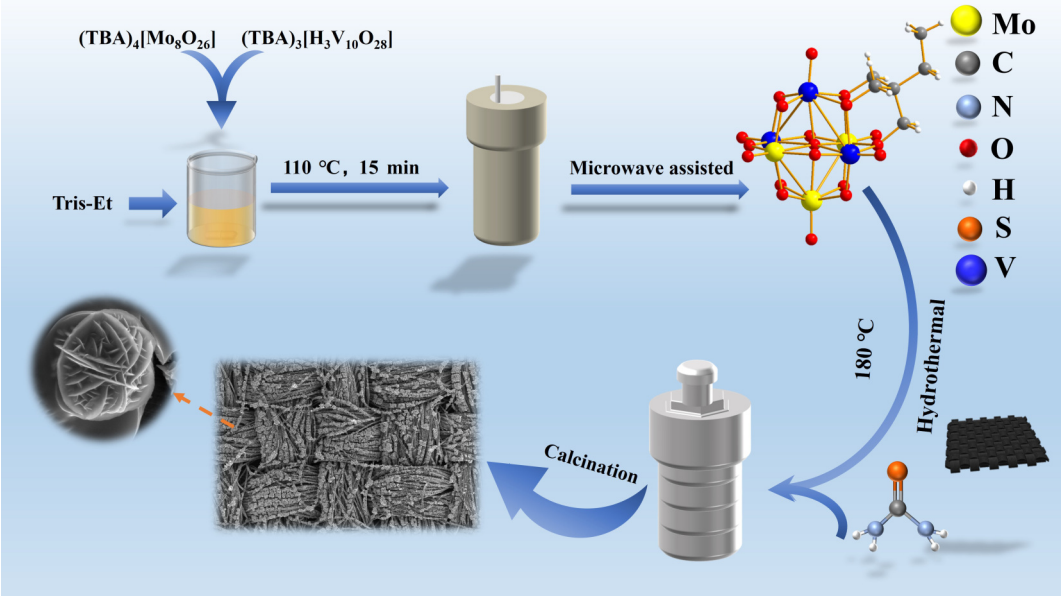

Scheme 1 Synthesis of MoS_2-V_2O_5@CC.

thiourea was used as the sulfur source, and CC was used as the conductive substrate. The MoS_2-V_2O_5@CC composite catalyst was prepared via a one-step hydrothermal method. Its HER performance was investigated using an electrochemical test system.

3.1 Synthesis and characterization of Mo_3V_3

The Fourier transform infrared (FT-IR) spectra of the Tris-Et-functionalized Mo_3V_3 cluster are shown in Fig. 1. The characteristic peaks of the POM framework are observed at 964.76 (s), 949.70 (vs), 935.59 (s), 882.98 (w), 812.45 (vs), and 738.66 (m). Among these, the absorption peaks at 964.76, 949.70, and 935.59 cm^{-1} are assigned to the terminal Mo=O and V=O stretching vibrations. The characteristic absorption peaks at 882.98, 812.45, and 738.66 cm^{-1} are attributed to the bridging V–O–V, V–O–Mo, and Mo–O–Mo vibrations. The absorption peak at 1061.05 cm^{-1} (vs), which corresponds to the C–O stretching vibration of the organic Tris-Et ligand, shows a slight shift compared to the free ligand (at 1058.29 cm^{-1}), indicating M–O–C bond formation and confirming the coordination of the ligand to the POM core [27]. The peaks at 2963.63–2875.21 cm^{-1} are assigned to the C–H stretching vibrations from both the coordinated Tris-Et ligand and the tetrabutylammonium bromide cation, further confirming the successful functionalization. ^{1}H nuclear magnetic resonance (NMR) spectroscopy (Fig. S1 in the Electronic Supplementary Material (ESM)) provided further confirmation of the compound's structure by revealing the positions and integration of the proton signals, which are in good agreement with the proposed structure and confirm the successful synthesis of the Tris-Et-Mo_3V_3 cluster.

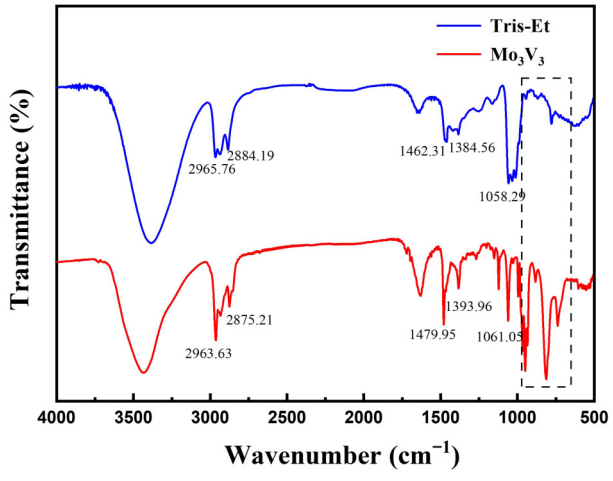

Figure 1 FT-IR spectra of Tris-Et and Mo_3V_3.

Single-crystal X-ray diffraction analysis (Tables S1–S3 in the Electronic Supplementary Material (ESM)) revealed that the core of the Mo_3V_3 cluster crystallized in the *Pbca* space group. The unit cell parameters are as follows: a = 15.6478(4) Å, b = 17.7185(6) Å, c = 37.3395(10) Å, and $\alpha = \beta = \gamma = 90°$. The structure comprises a preorganized, heterometallic core with a fixed Mo:V ratio of 1:1. This well-defined and stoichiometrically precise inorganic core indicates the success of our precursor design strategy.

3.2 Selective behavior of vanadium in the V_{10} precursor

V_{10} was used as the research model to investigate the selectivity of vanadium-based POMs toward oxygen and sulfur under hydrothermal conditions. Following the same preparation steps of MoS_2-V_2O_5@CC, with a metal-to-sulfur (M:S) feed ratio of 1:4.17 [28], the product was obtained via hydrothermal reaction and subsequent calcination. The product was systematically characterized by X-ray photoelectron spectroscopy (XPS) and X-ray diffraction (XRD).

In the XPS survey spectrum of the product (Fig. 2(a)), only V, C, and O were detected. The signal for S was very weak and almost negligible. This result is in good agreement with the S 2p spectrum (Fig. 2(b)), which shows messy signals and no distinct characteristic peaks. This indicates that no stable sulfur-containing species were formed under the experimental conditions.

Further analysis of the high-resolution spectra for O 1s and V 2p (Fig. 2(c)) revealed peaks at binding energies of 516.3 and 523.4 eV, which are attributed to V^{4+}. The peaks at 517.6 and 524.7 eV correspond to V^{5+} [29]. In the O 1s spectrum, the peaks at 530.2, 531.5, and 532.7 eV are assigned to the V–O, C=O, and C–O bonds, respectively. [30].

Furthermore, the C 1s spectrum (Fig. 2(d)) shows characteristic peaks for C–O and O=C–O at 286.2 and 288.9 eV, respectively

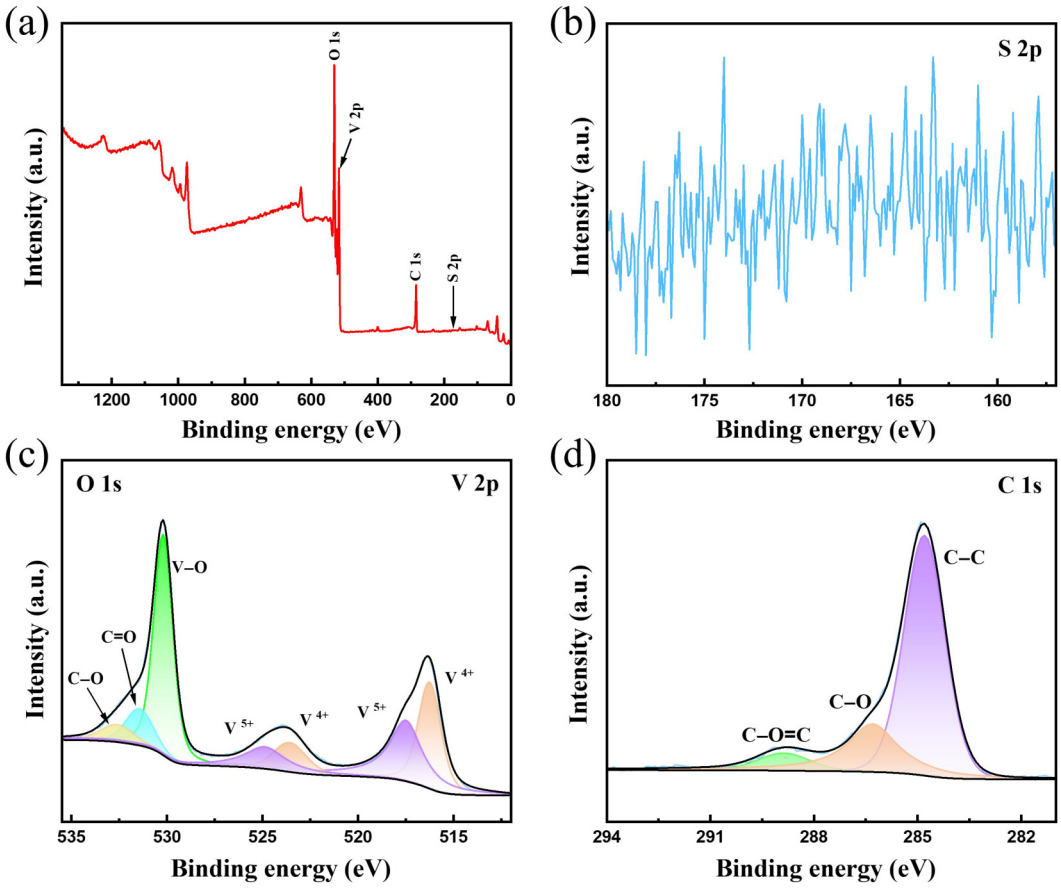

Figure 2 XPS spectra of V_2O_5@CC: (a) full spectrum; (b) S 2p; (c) O 1s and V 2p; (d) C 1s.

[31], which can be attributed to the oxygen-containing functional groups on the activated CC substrate. These functional groups can act as active anchoring sites for vanadium oxide precursors. They facilitate the formation of V_2O_5 and promote the oriented growth of V_2O_5 nano-arrays as well as their strong attachment to the substrate [32].

The above characterization results consistently indicate that under hydrothermal conditions, vanadium-based POMs exhibit a considerably higher selectivity for oxygen over sulfur, leading to stable formation of vanadium oxides. This conclusion provides an important experimental basis and theoretical support for subsequent studies on directed transformation of Mo_3V_3 into MoS_2 and V_2O_5 in hydrothermal systems.

3.3 Characterization of the composites

XRD was used to identify the phase and composition of the catalysts (Fig. 3). The successful synthesis of MoS_2 and V_2O_5 phases was confirmed after comparing the results with standard cards (PDF#37-1492 and PDF#41-1426).

In the case of MoS_2-V_2O_5@CC, although its overall crystallinity is low, the main diffraction features of both phases (MoS_2 and V_2O_5) are preserved. The diffraction peaks at 2θ = 13.6°, 32.8°, and 59.7° are assigned to the (002), (100), and (110) crystal planes of MoS_2, respectively. Moreover, the diffraction peaks at 2θ = 15.2°, 25.4°, 26.6°, 36.3°, 41.4°, and 54.4° correspond to the (200), (201), (110), (211), (002), and (220) planes of V_2O_5, respectively.

Notably, the diffraction peaks assigned to the (211), (002), and (220) crystal planes of V_2O_5 all shifted to the left (lower angles) by 0.2°–0.6°. According to Bragg's law, this shift directly signifies an

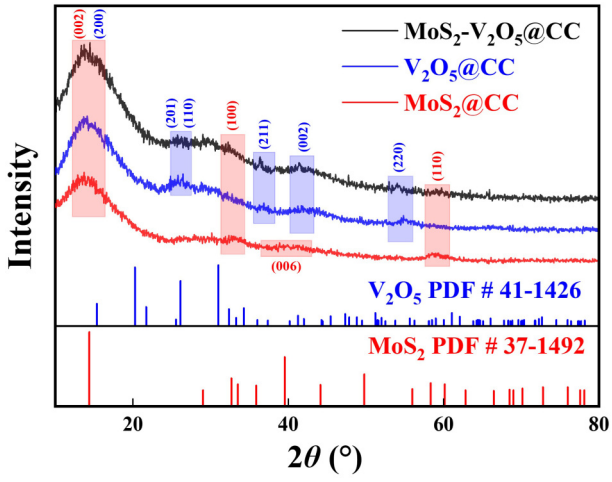

Figure 3 XRD patterns of the catalysts.

increase in the interplanar spacing of V_2O_5, indicating the occurrence of lattice expansion. This may be due to the substitution of the smaller V^{5+} in the lattice by larger Mo^{4+} [18, 33]. Similar phenomena of lattice expansion and diffraction peak shifts induced by ion doping have been reported in various transition metal oxide systems [34]. This localized cation substitution leads to lattice distortion and may considerably modulate the electronic structure of the material, thereby contributing to enhanced interfacial charge transfer efficiency [35]. These results further confirm the formation of a strongly coupled heterojunction interface between MoS_2 and V_2O_5 via ionic-scale interactions. This result suggests the formation

of a tight heterojunction interface with strong electronic interactions between MoS_2 and V_2O_5.

XPS was used to further study the chemical composition and elemental valence states of MoS_2-V_2O_5@CC. The full XPS spectra of the three samples (Fig. 4(a)) clearly show their distinct elemental signatures: MoS_2-V_2O_5@CC exhibits peaks for all constituent elements (C, Mo, O, V, S); MoS_2@CC shows peaks for C, Mo, O, and S; and V_2O_5@CC shows peaks for C, V, and O.

The Mo 3d spectrum of MoS_2-V_2O_5@CC (Fig. 4(b)) shows that Mo exists in two oxidation states. The characteristic peaks at binding energies of 232.5 and 229.5 eV correspond to the $3d_{3/2}$ and $3d_{5/2}$ orbitals of Mo^{4+}, respectively. This indicates that Mo in the catalyst mainly exists in the +4 oxidation state. Two weak characteristic peaks were observed at 235.8 and 232.9 eV, corresponding to the characteristic signals of Mo^{6+} in MoO_3. This indicates that a small amount of MoS_2 was oxidized during synthesis [36]. In addition, the characteristic peak at 226.7 eV corresponds to the S 2s orbital signal from the Mo–S bond, confirming the bonding between Mo and S [37]. For S 2p (Fig. 4(c)), the characteristic peaks at 163.7 and 162.5 eV correspond to the $2p_{1/2}$ and $2p_{3/2}$ orbitals of S^{2-}, respectively [38]. This further verifies the presence of the MoS_2 phase in the catalyst.

Figure 4(d) shows the XPS spectrum of V 2p. The characteristic peaks at 524.3 and 517.1 eV correspond to the $2p_{1/2}$ and $2p_{3/2}$ orbitals of V^{5+}, respectively. The peaks at 522.9 and 516.0 eV are attributed to the $2p_{1/2}$ and $2p_{3/2}$ orbitals of V^{4+}, respectively. Notably, the proportion of V^{4+} in MoS_2-V_2O_5@CC (0.32) is lower than that in V_2O_5@CC (0.45).

The formation of V^{4+} can be attributed to a multistage reduction mechanism during synthesis. First, the weak reducing environment generated by the decomposition of thiourea under hydrothermal conditions initiate the preliminary surface reduction of V^{5+} species. Next, high-temperature calcination in an H_2/Ar atmosphere provides a strong global reducing environment, effectively suppressing reoxidation and promoting deeper reduction. Moreover, the intimate contact between the active material and the conductive CC substrate offers an interfacial reduction effect. The CC acts as a conductive carrier, facilitating electron transfer and potentially assisting and stabilizing the conversion of V^{5+} to V^{4+} through direct interfacial interactions under the reducing atmosphere and heating conditions [39]. The formation of this V^{4+}/V^{5+} mixed-valence structure according to the principle of charge balance inevitably accompanies the generation of oxygen vacancies within the lattice [40–42]. Notably, the resulting mixed-valence V_2O_5 structure typically exhibits greater intrinsic electrochemical activity, more efficient ion diffusion capability, and superior electronic conductivity than its single-valence counterpart [29, 43]. Therefore, the observed stable V^{4+} species and the resulting structural advantages are a comprehensive outcome of the sequential action and synergistic effects of the hydrothermal synthesis of the precursor, reductive atmosphere annealing, and interfacial-assisted reduction by the carbon substrate. Moreover, this structural advantage is directly demonstrated by the similar proportion of V^{4+} in the material after 100 h of continuous electrolysis testing (0.38) and in its initial state (0.32) (Fig. S6 in the ESM), indicating the excellent stability of its mixed-valence structure under reaction conditions.

Compared with the single-component MoS_2@CC and

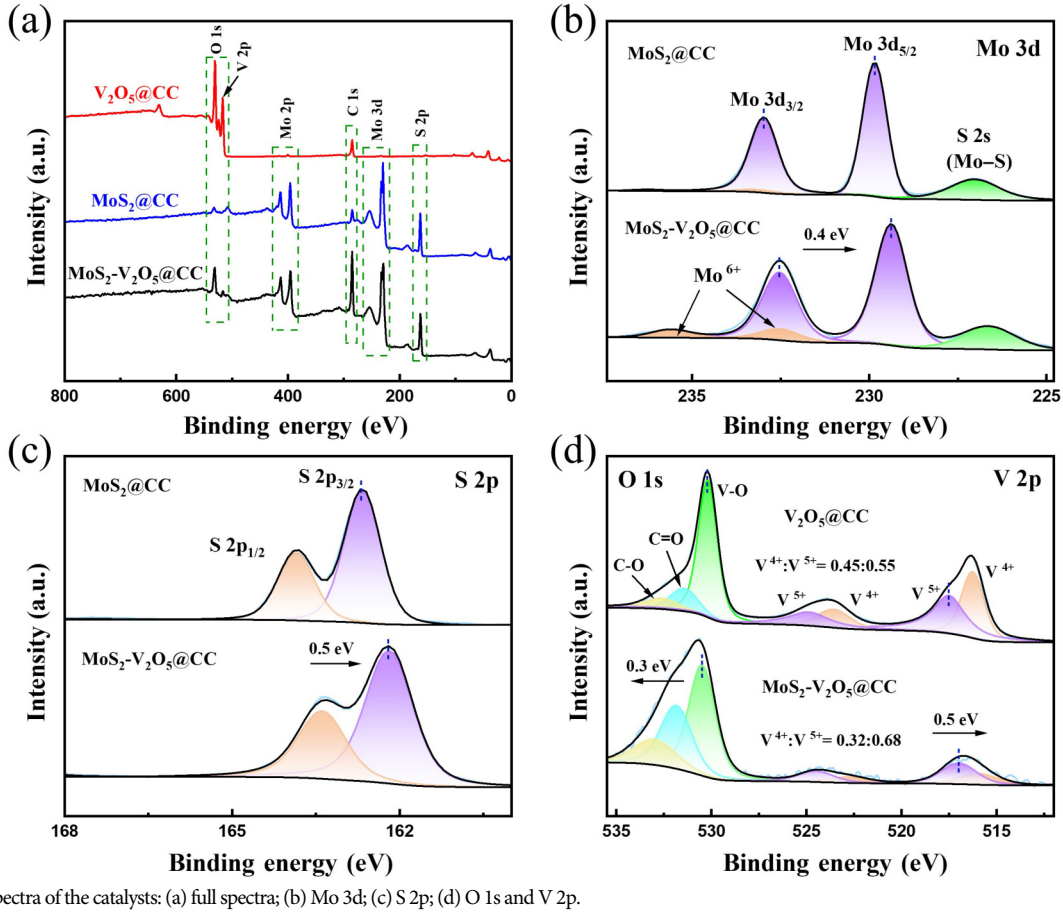

Figure 4 XPS spectra of the catalysts: (a) full spectra; (b) Mo 3d; (c) S 2p; (d) O 1s and V 2p.

V_2O_5@CC, MoS_2-V_2O_5@CC exhibits a distinct trend in elemental binding energy shifts: the Mo 3d, S 2p, and V 2p peaks all shift toward lower binding energies, whereas the O 1s peak shifts toward higher binding energy. This systematic shift reveals directional electron transfer from MoS_2 to V_2O_5 across the heterointerface, which is accompanied by charge redistribution within the V_2O_5 lattice. This phenomenon confirms the lattice expansion of V_2O_5 observed in the XRD analysis. Both pieces of evidence point toward the doping of the V_2O_5 lattice by Mo^{4+}. The substitution of V^{5+} by the larger Mo^{4+} causes lattice expansion. Simultaneously, Mo^{4+} acts as an electron donor, injecting electrons into V_2O_5, which increases the electron density at the V sites, leading to an overall decrease in the binding energy. This doping-induced strong electronic interaction optimizes the interfacial charge distribution, which enhances the electrocatalytic performance [44, 45]. The morphology of the catalyst was systematically characterized using scanning electron microscopy (SEM) at different magnifications. As shown in Fig. 5(a), uniformly distributed nanocluster structures were formed on the CC of MoS_2-V_2O_5@CC. Compared with the V_2O_5@CC and MoS_2@CC (Figs. S2(a)–S2(d) in the ESM), V_2O_5 in the composite material appears as a relatively continuous film completely encapsulating the carbon fiber substrate. The film is also closely coupled with the three‐dimensionally grown MoS_2 nanoflowers, jointly constructing a stable core–shell heterostructure (Figs. 5(b)–5(d)). This V_2O_5 film functions as a "conductive glue," effectively enhancing the interfacial bonding between carbon fibers and composite components, thereby improving the structural stability of the material while providing abundant catalytic active sites [46].

The microstructure and phase characteristics of the material were analyzed using transmission electron microscopy (TEM). As shown in Figs. 6(a)–6(c) and Fig. S3 in the ESM, the characteristic crystal planes of V_2O_5, such as (211), (002), and (200), and of MoS_2, such as (006), (100), and (002), were identified based on the analysis of lattice fringe spacings. These results are in good agreement with the XRD analysis and further confirm the successful preparation of MoS_2-V_2O_5@CC. The overall crystallinity of the material is low, in which the central parts of the nanosheets are mostly amorphous and the (002) crystal planes of MoS_2 are more distinct at the edges. These often overlap with the V_2O_5 crystal planes, causing the (002) interplanar spacing to be slightly larger than the standard value. This further indicates a strong interaction between the two phases, suggesting that some V dopants have entered the MoS_2 lattice.

Furthermore, energy-dispersive X-ray spectroscopy (EDS) (Fig. S4 in the ESM) was used to investigate the elemental distribution and composition. The results show that a small amount of V (1.23%) and a large amount of Mo (19.18%) are uniformly dispersed within the MoS_2-V_2O_5@CC heterostructure. This low vanadium content may be attributed to its partial loss during synthesis, as the thiourea-derived alkaline environment promotes the formation of soluble vanadate ions.

All characterization results confirm each other. They collectively indicate that the POM precursor induces dual doping and composite formation between MoS_2 and V_2O_5 at the atomic scale. As a result, a tight heterojunction interface with strong electronic interactions is successfully formed.

3.4 Electrocatalytic HER performance and stability

To compare the effect of V_2O_5 composite on the overall catalytic performance, we investigated the HER behavior of CC, V_2O_5@CC, MoS_2@CC, and MoS_2-V_2O_5@CC in KOH (1 M) using a three-electrode system. As shown in Fig. 7(a), the overpotentials at 100 $mA{\cdot}cm^{-2}$ for bare CC, V_2O_5@CC, MoS_2@CC, and MoS_2-V_2O_5@CC were 715, 808, 312, and 244 mV, respectively. The performance of MoS_2-V_2O_5@CC was considerably higher than that of the single-component catalysts. This indicates that the composite of V_2O_5 and MoS_2 can considerably enhance the HER activity.

The electrochemical active area of each sample was evaluated by measuring the double-layer capacitance (C_{dl}) using CV (Fig. S5 in the ESM) [47]. As shown in Fig. 7(b), the C_{dl} values for CC, V_2O_5@CC, MoS_2@CC, and MoS_2-V_2O_5@CC were 1.09, 11.07, 37.45, and 159.36 $mF{\cdot}cm^{-2}$, respectively. This demonstrates that the incorporation of V_2O_5 can considerably increase the number of active sites in the MoS_2-based material, which is in good agreement with our previous conjecture.

The Tafel slope, which is quantified using the Tafel equation, is commonly used to evaluate HER kinetics [36]. As shown in Fig. 7(c), the Tafel slope of MoS_2-V_2O_5@CC (91.44 $mV{\cdot}dec^{-1}$) was

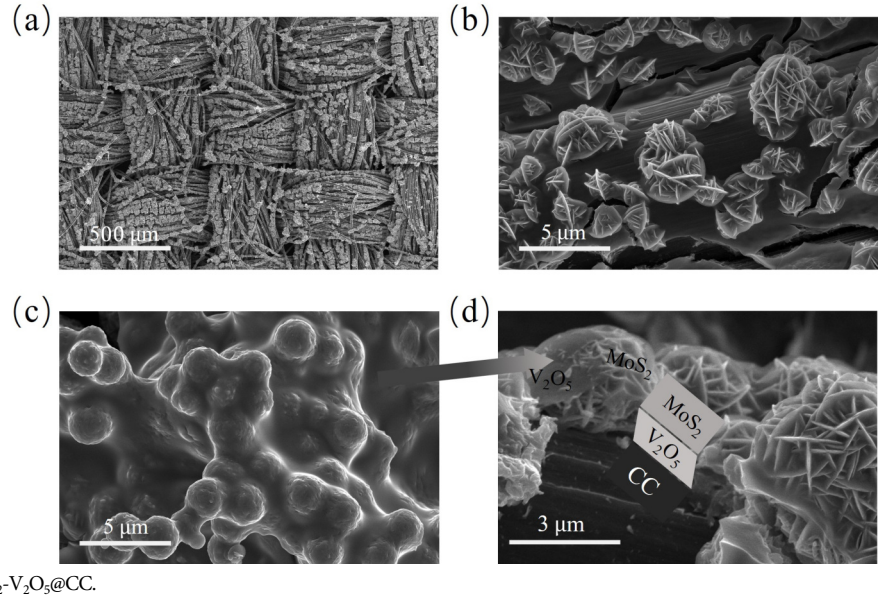

Figure 5 SEM images of MoS_2-V_2O_5@CC.

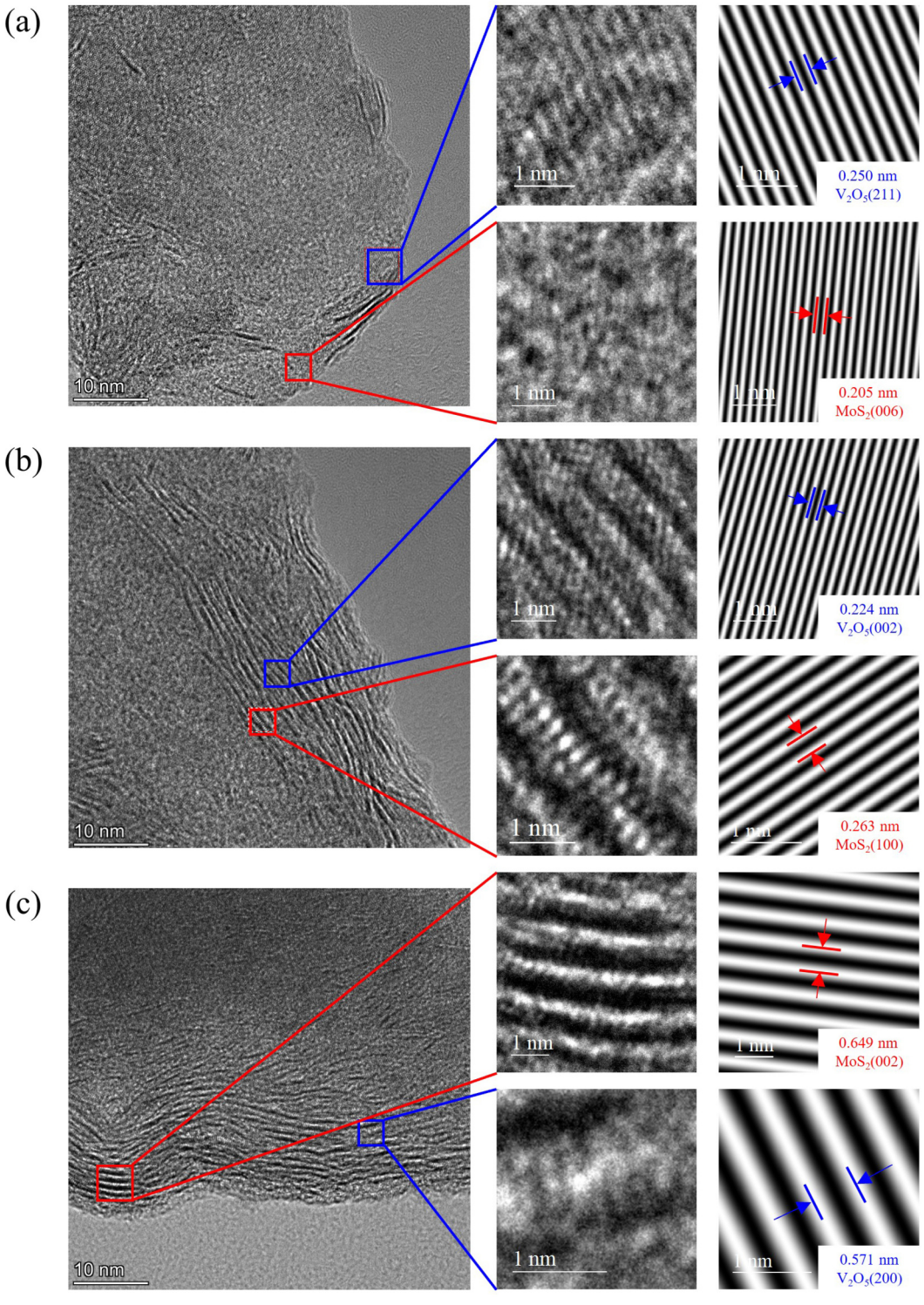

Figure 6 TEM images of MoS_2-V_2O_5@CC.

slightly smaller than that of MoS_2@CC (93.34 mV·dec^{-1}) and considerably smaller than those of V_2O_5@CC (301.35 mV·dec^{-1}) and CC (148.53 mV·dec^{-1}). Although V_2O_5@CC itself exhibits poor kinetics, its composite with MoS_2@CC did not alter the fundamental HER pathway (Volmer–Heyrovsky) but slightly improved the reaction kinetics. This enhancement can be mainly attributed to the subtle optimization of the interfacial electronic structure, which effectively facilitates the Heyrovsky step, thereby boosting the overall catalytic activity of the composite material [26, 48].

Nyquist plots were obtained using EIS at an overpotential of 100 mV (Fig. 7(d)). Comparing the diameters of the semicircles, the charge transfer resistance (R_{ct}) of the materials increases in the following order: MoS_2-V_2O_5@CC (22.9 Ω) < MoS_2@CC (57.3 Ω) < V_2O_5@CC (181.0 Ω) < CC (192.1 Ω). Thus, MoS_2-V_2O_5@CC has the lowest charge transfer resistance, confirming that the charge

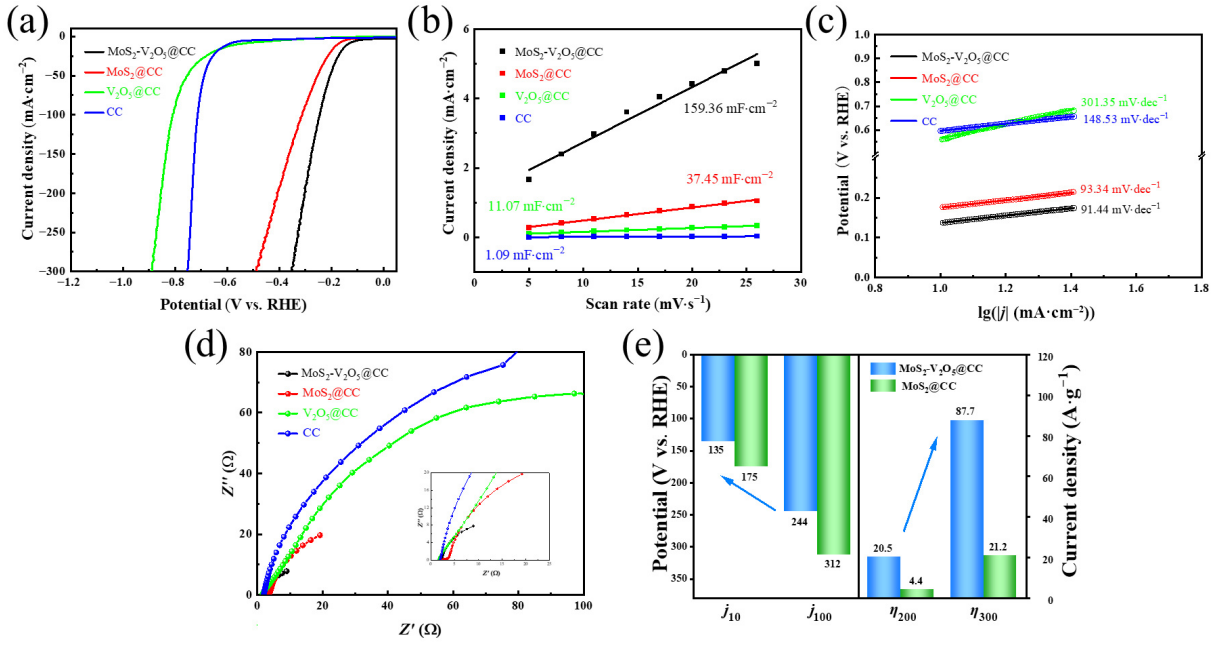

Figure 7 HER performance of the catalysts in 1 M KOH: (a) LSV curves; (b) C_{dl} plots; (c) Tafel plots; (d) Nyquist plots; (e) mass activity.

transfer efficiency of the composite is effectively enhanced compared to those of the single components.

Mass activity is a key metric for evaluating the intrinsic catalytic performance of materials [49]. Herein, the mass activities of the MoS_2-V_2O_5@CC composite and the pure MoS_2@CC sample were compared at overpotentials of 200 and 300 mV (Fig. 7(e)). The results show that, compared to pure MoS_2, MoS_2-V_2O_5@CC exhibits a large enhancement in mass activity, demonstrating the synergistic enhancement effect between the two components. To assess the overall performance advantage of MoS_2-V_2O_5@CC, its key electrochemical metrics were compared with those of recently reported V-doped MoS_2 or V_2O_5-MoS_2 composite electrocatalysts (Table S4 in the ESM).

The cycling stability of the catalysts was evaluated by comparing the LSV curves before and after 5000 CV cycles. Figures 8(a)–8(c) show the overpotential shift at 100 mA·cm^{-2} after 5000 cycles. Compared to the shifts of MoS_2@CC and V_2O_5@CC (6 and 7 mV, respectively), the overpotential of MoS_2-V_2O_5@CC shifted by only 1 mV, demonstrating excellent cycling stability.

The long-term stability of MoS_2-V_2O_5@CC was further evaluated by chronoamperometry (*I*–*T*). As shown in Fig. 8(d), MoS_2-V_2O_5@CC retained 80% of its initial current density after a 100-h stability test at a high current density (100 mA·cm^{-2}). The structural changes of the catalyst after the *I*–*T* test under harsh alkaline hydrogen evolution conditions were systematically analyzed using XPS, XRD, and SEM (Figs. S6(a)–S6(g) in the ESM). The

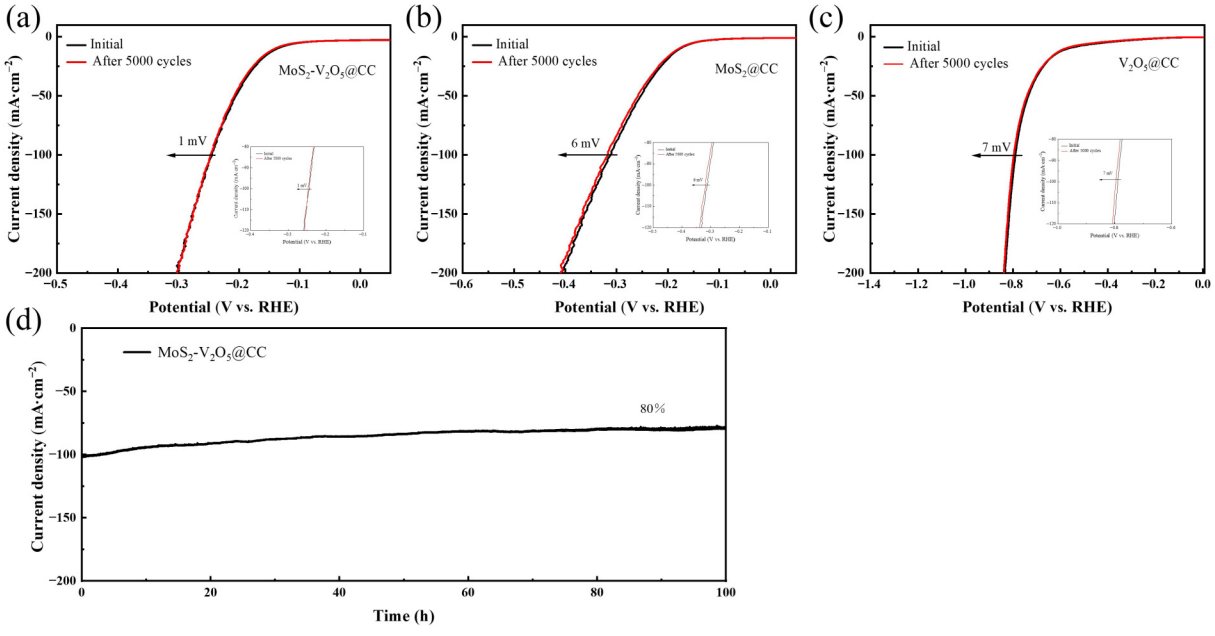

Figure 8 (a)–(c) Polarization curves of the catalysts before and after 5000 CV cycles. (d) 100 h *I*–*T* tests of MoS_2-V_2O_5@CC over 100 mA·cm^{-2}.

characterization results revealed the dynamic structural evolution of the material: A small fraction of Mo^{4+} was oxidized to Mo^{6+} during the reaction, the main crystalline phase remained intact with only a slight decrease in crystallinity, and vanadium species underwent partial dissolution. However, the multidimensional conductive network of the material was preserved. Despite these changes, the material maintained approximately 80% of its initial activity, with a performance decay considerably lower than that of comparable catalysts. This confirms the excellent structural stability of the material and its suitability for practical operating conditions. This outstanding stability can be attributed to the tight core–shell heterostructure synergistically constructed from CC, V_2O_5, and MoS_2. This structure effectively inhibits the hydrolysis of V_2O_5 in alkaline media and provides a stable mechanical and conductive framework for charge transport and mass transfer.

The one-pot hydrothermal method based on POM precursors proposed in this work offers huge advantages such as its simple operation, streamlined process, and the resultant materials with superior catalytic performance. However, the atomic utilization of vanadium in the proposed method is lower than that in the preparation routes reported in the literature owing to the uncontrollable dissolution of vanadium species in the current hydrothermal reaction environment. This is a key problem that should be addressed during future optimization of this synthesis system.

4 Conclusions

Herein, we proposed a simple one-pot hydrothermal method using a POM precursor to grow a MoS_2-V_2O_5 composite with an intimate heterointerface *in situ* on CC. The electrocatalytic HER performance was investigated. Electrochemical studies demonstrated that MoS-V_2O_5@CC exhibits considerably higher activity and stability than MoS_2@CC and V_2O_5@CC. This superior performance is attributed to the following factors: 1) The POM precursor induces dual doping and composite formation between MoS_2 and V_2O_5 at the atomic scale, creating an intimate heterointerface with strong electronic interactions. 2) The unique core–shell structure, in which the V_2O_5 film encapsulates MoS_2 nanoflowers, provides abundant active sites and enhances the material mechanical stability. 3) The V^{4+}/V^{5+} mixed-valence states and oxygen vacancies considerably enhance the intrinsic conductivity and operational durability of the material.

Electronic Supplementary Material: Supplementary material (crystal data, XPS, XRD, and SEM of catalysts) is available in the online version of this article at https://doi.org/10.26599/POM.2026.9140125.

CCDC 2294653 contain the supplementary crystallographic data for this paper. These data can be obtained free of charge via www.ccdc.cam.ac.uk/structures/, or by emailing data_request@ccdc.cam.ac.uk, or by contacting The Cambridge Crystallographic Data Centre, 12 Union Road, Cambridge CB2 1EZ, UK; fax: +44 1223 336033.

Data availability

All data needed to support the conclusions in the paper are presented in the manuscript and the Electronic Supplementary Material. Additional data related to this paper may be requested from the corresponding author upon request.

Acknowledgements

The authors are grateful to the Institute of POM-based Materials, National Natural Science Foundation of China (No. 21271068), and National College Students' Innovation and Entrepreneurship Training program (Nos. 20250100076).

Declaration of competing interest

The authors declare that they have no known competing financial interests or personal relationships that could have appeared to influence the work reported in this paper.

Author contribution statement

S. Z. S: Investigation, software, writing – original draft. X. F.: Data curation, investigation. J. S.: Formal analysis. Q. S. C.: Formal analysis. S. Y. O.: Visualization. S. X. Z.: Investigation. Y. H. L.: Investigation. P. F. W.: Supervision, writing – review & editing, funding acquisition.

Use of AI statement

None.

References

[1] Molecular dinner invitations. *Sci. Signal.* **2003**, *2003*, tw468–337.
[2] Dresselhaus, M. S.; Thomas, I. L. Alternative energy technologies. *Nature* **2001**, *414*, 332–337.
[3] Huang, Y. C.; Shen, H. W.; Wang, L. M.; Xie, H. X.; Liang, D.; Xing, J. S.; Chen, L. L.; Dai, X. D.; Zhou, Y.; Liao, M. H. et al. Achieving ultra-stable hydrogen evolution at 2000 mA cm^{-2} via a hierarchical Pt electrocatalyst with dual charge/mass transfer networks. *Adv. Powder Mater.* **2026**, *5*, 100389.
[4] Liu, Z. Y.; Chen, L. L.; Huang, S. X.; Liu, M. Q.; Ye, Q. M.; Huang, Y. C. A strongly coupled Pt-W_2N heterostructure embedded in porous carbon nanoflowers for seawater electrolysis. *Sci. China Mater.* **2025**, *68*, 3626–3637.
[5] Cao, Y. Roadmap and direction toward high-performance MoS_2 hydrogen evolution catalysts. *ACS Nano* **2021**, *15*, 11014–11039.
[6] Nisar, T.; Asghar, M. A.; Siddique, A. N.; Haider, A.; Furlan, K. P.; Wagner, V. Facile spin-coated MoS_2 thin films from a single-source precursor for HER activity. *ACS Appl. Energy Mater.* **2025**, *8*, 9497–9505.
[7] Kibsgaard, J.; Chen, Z. B.; Reinecke, B. N.; Jaramillo, T. F. Engineering the surface structure of MoS_2 to preferentially expose active edge sites for electrocatalysis. *Nat. Mater.* **2012**, *11*, 963–969.
[8] Wang, H.; Xiao, X.; Liu, S. Y.; Chiang, C. L.; Kuai, X. X.; Peng, C. K.; Lin, Y. C.; Meng, X.; Zhao, J. Q.; Choi, J. et al. Structural and electronic optimization of MoS_2 edges for hydrogen evolution. *J. Am. Chem. Soc.* **2019**, *141*, 18578–18584.
[9] You, M. Y.; Zhang, W. J.; Yan, X. H.; Jiang, H.; Miao, J. Y.; Li, Y. L.; Zhou, W. D.; Zhu, Y. H.; Cheng, X. N. V_2O_5 nanosheets assembled on 3D carbon fiber felt as a free-standing electrode for flexible asymmetric supercapacitor with remarkable energy density. *Ceram. Int.* **2021**, *47*, 3337–3345.
[10] Irshad, A.; Zulfiqar, S.; Aalothman, Z. A.; Shakir, I.; Warsi, M. F.; Cochran, E. W. Synergy of zero-dimensional carbon dots decoration on the one-dimensional architecture of Ag-doped V_2O_5 for supercapacitor and overall water-splitting applications. *Fuel* **2024**, *362*, 130705.
[11] Peng, C. Y.; Jin, M. M.; Han, D.; Liu, X.; Lai, L. F. Structural engineering of V_2O_5 nanobelts for flexible supercapacitors. *Mater. Lett.* **2022**, *320*, 132391.

[12] Mohan, M.; Shetti, N. P.; Aminabhavi, T. M. Phase dependent performance of MoS_2 for supercapacitor applications. *J. Energy Storage* **2023**, *58*, 106321.
[13] Ghosh, A.; Islam, M. S.; Rahman, M. K.; Buian, M. F. I.; Hassan, A. A.; Alrafai, H. A.; Abdelrahim, S. K. A. A theoretical investigation of MoS_2-based solar cells with CdS electron transport layer and V_2O_5 hole transport layer for boosting performance. *Mater. Sci. Eng: B* **2024**, *307*, 117521.
[14] Hassan, H.; Mumtaz, S.; Iqbal, M. W.; Afzal, A. M.; Yaseen, T.; Sunny, M. A.; Mohammad, S.; Alotaibi, N. H.; Manzoor, M. Revolutionizing energy: Vanadium pentoxide (V_2O_5) and molybdenum disulfide (MoS_2) composite incorporated with GQDs as a dual-purpose material for supercapacitors and hydrogen evolution. *Solid State Ionics* **2025**, *421*, 116784.
[15] Nadeem, M. T.; Aqeel, R.; Zafar, A.; Nisar, A.; Khan, M. I.; Ahmad, M. Synergic effect of a MoS_2-V_2O_5 heterostructure as an advanced catalyst for photocatalytic degradation of methylene blue. *New J. Chem.* **2025**, *49*, 1171–1181.
[16] Prashant; Singh, N.; Kumar, A.; Dhiman, V.; Kour, S.; Sharma, A. L.; Sharma, R.; Kondal, N. Optimized MoS_2-V_2O_5 nanocomposites: Unveiling superior structural, morphological, and electrochemical properties for advanced energy storage applications. *J. Alloys Compd.* **2025**, *1017*, 178969.
[17] Jameel, M. H.; Yasin, A.; Samia, N.; Hilmi Bin Mayzan, M. Z.; Sufi bin Roslan, M.; Bin Agam, M. A.; Althubeiti, K.; Aljohani, M. Modification in structural, optical and morphological properties of hydrothermally synthesized 2D layered structured $MoS_{2(x)}V_2O_{5(1-x)}$(X=1–5%) nanocomposites for photocatalytic application. *Results Eng.* **2024**, *24*, 103010.
[18] Haldar, K. K.; Ahmed, I.; Biswas, R.; Mete, S.; Patil, R. A.; Ma, Y. R. Efficient MoS_2/V_2O_5 electrocatalyst for enhanced oxygen and hydrogen evolution reactions. *Electrocatalysis* **2023**, *14*, 624–635.
[19] Syed, W. A.; Kakarla, A. K.; Bandi, H.; Shanthappa, R.; Yu, J. S. Improved rate and cycling capability of V_2O_5@MoS_2 nanocomposites as an advanced cathode material for rechargeable aqueous zinc-ion batteries. *Sustain. Mater. Technol.* **2024**, *40*, e00968.
[20] Alahmadi, M.; Mohamed, W. S.; Zhukov, A.; Salaheldeen, M.; Alsaedi, W. H.; Alhashmialameer, D.; Al-Ghamdi, K.; Abu-Dief, A. M. One-step hydrothermal synthesis of flower-like MoS_2/VS_2 nanocomposite for biomedical applications. *Inorg. Chem. Commun.* **2023**, *157*, 111336.
[21] Zhang, Y.; Liu, Y. F.; Wang, D.; Liu, J. C.; Zhao, J. W.; Chen, L. J. State-of-the-art advances in the syntheses, structures, and applications of polyoxometalate-based metal-organic frameworks. *Polyoxometalates* **2023**, *2*, 9140017.
[22] Zang, D. J.; Wang, H. Q. Polyoxometalate-based nanostructures for electrocatalytic and photocatalytic CO_2 reduction. *Polyoxometalates* **2022**, *1*, 9140006.
[23] Sanwal, P.; Raza, A.; Miao, Y. X.; Lumbers, B.; Li, G. Advances in coinage metal nanoclusters: From synthesis strategies to electrocatalytic performance. *Polyoxometalates* **2024**, *3*, 9140057.
[24] Xu, S. Y.; Wang, P.; Zhang, B. W.; Wang, C.; Low, J.; Ivanov, V. K.; Zhang, Z. M. Nickel-substituted polyoxometalate-CdS single-cluster photocatalysts for efficient plastic waste degradation coupled with H_2 production. *Polyoxometalates* **2025**, *4*, 9140096.
[25] Cai, Q. M.; Gao, R. L.; Wang, Y. F.; Xing, J. S.; Zhang, Q. Y.; Zhu, M. Z.; Qin, X. Y.; Liao, M. H.; Huang, Y. C. Ruthenium containing polyoxometalates: From synthesis, structures, properties to functional applications. *Polyoxometalates* **2025**, *4*, 9140083.
[26] Zeb, Z.; Huang, Y. C.; Chen, L. L.; Zhou, W. B.; Liao, M. H.; Jiang, Y. Y.; Li, H. T.; Wang, L. M.; Wang, L.; Wang, H. et al. Comprehensive overview of polyoxometalates for electrocatalytic hydrogen evolution reaction. *Coord. Chem. Rev.* **2023**, *482*, 215058.
[27] Karoui, H.; Ritchie, C. Microwave-assisted synthesis of organically functionalized hexa-molybdovanadates. *New J. Chem.* **2018**, *42*, 25–28.
[28] Shu, S. Z.; Zhu, D. L.; Wang, X. J.; Sun, J.; Wang, J. N.; Ling, Q.; Zhou, Z. L.; Chen, Y. J.; Wu, P. F. High-performance Co_4S_3-MnS-MoS_2@CC catalysts for the hydrogen evolution reaction. *J. Mater. Chem. A* **2025**, *13*, 17740–17747.
[29] Ahirrao, D. J.; Mohanapriya, K.; Jha, N. V_2O_5 nanowires-graphene composite as an outstanding electrode material for high electrochemical performance and long-cycle-life supercapacitor. *Mater. Res. Bull.* **2018**, *108*, 73–82.
[30] Chen, B.; Wei, J.; Qiao, X. Y.; Liang, D.; Ji, Y. X. V_2O_5 plates anchored in CNTS composite materials with a network structure as polysulfide capture for lithium-sulfur battery. *Ceram. Int.* **2022**, *48*, 32348–32356.
[31] Chen, H. P.; Meng, C. F.; Jiao, Z. C.; Yuan, A. H.; Zhou, H. Amphiphilic dodecanoic monolayer protects zinc anode from water-involved side reactions. *Energy Fuels* **2025**, *39*, 4069–4078.
[32] Zhou, X.; Chen, Q.; Wang, A. Q.; Xu, J.; Wu, S. S.; Shen, J. Bamboo-like composites of V_2O_5/polyindole and activated carbon cloth as electrodes for all-solid-state flexible asymmetric supercapacitors. *ACS Appl. Mater. Interfaces* **2016**, *8*, 3776–3783.
[33] Anson, A.; Mondal, D.; Biswas, V.; Urs, K.; Kamble, V. Suppressed polaronic conductivity induced sensor response enhancement in Mo doped V_2O_5 nanowires. *J. Appl. Phys.* **2023**, *133*, 194505.
[34] Zhu, M.; Gao, J.; Zhang, C. La-doping-induced lattice strain and electronic state modulation in RuO_2 for electrocatalytic oxygen evolution in acidic solutions. *Inorg. Chem.* **2025**, *64*, 4571–4579.
[35] Liu, T.; Fang, C. J.; Yu, B. S.; You, Y.; Niu, H. H.; Zhou, R.; Zhang, J. J.; Xu, J. Vanadium-doping in interlayer-expanded MoS_2nanosheets for the efficient electrocatalytic hydrogen evolution reaction. *Inorg. Chem. Front.* **2020**, *7*, 2497–2505.
[36] Chen, L. L.; Huang, Y. C.; Wang, J. J.; Liao, M. H.; Huang, S. X.; Cai, H. Q.; Wang, L.; Zhao, L. M.; Pu, N.; Fan, Z. J. Platinum-dependent 2H-to-1T phases conversion of MoS_2 nanosheets growing on cross-interlocking porous carbon for boosting hydrogen evolution reaction. *Chem. Eng. J.* **2024**, *498*, 155060.
[37] Cheng, Y.; Zhao, C. C.; Wang, T. T.; Zhang, M.; Ru, S.; Deng, Y. K.; Wang, W. Y.; Wang, Y.; Song, Y. X.; Wei, Y. G. et al. Interfacial engineering of Cu_9S_5@MoS_2 p-n type heterojunction via *in situ* phase separation for highly efficient electrocatalytic oxidation of 5-hydroxymethylfurfural. *eScience*, in press, DOI: 10.1016/j.esci.2025.100507.
[38] Yap, F. M.; Loh, J. Y.; Ong, W. J. Synergistic integration of self-supported 1T/2H-WS_2 and nitrogen-doped rGO on carbon cloth for pH-universal electrocatalytic hydrogen evolution. *Nano Res.* **2024**, *17*, 1267–1280.
[39] Dönges, I.; Yadav, S.; Trouillet, V.; Schneider, J. J. Selective synthesis of 3D aligned VO_2 and V_2O_5 carbon nanotube hybrid materials by chemical vapor deposition. *Chem.—Eur. J.* **2024**, *30*, e202402024.
[40] Wang, Y. Q.; Zhang, Z. J. Oxygen deficient V_2O_5 nanorods for gas sensing. *Phys. E: Low-Dimens. Syst. Nanostruct.* **2011**, *43*, 1726–1729.
[41] Song, H. Q.; Zhang, C. P.; Liu, Y. G.; Liu, C. F.; Nan, X. H.; Cao, G. Z. Facile synthesis of mesoporous V_2O_5 nanosheets with superior rate capability and excellent cycling stability for lithium ion batteries. *J. Power Sources* **2015**, *294*, 1–7.
[42] Liang, X.; Gao, G. H.; Feng, S. Z.; Du, Y. C.; Wu, G. M. Synthesis and characterization of carbon supported V_2O_5 nanotubes and their electrochemical properties. *J. Alloys Compd.* **2019**, *772*, 429–437.
[43] Sun, G.; Ren, H.; Shi, Z. T.; Zhang, L.; Wang, Z.; Zhan, K.; Yan, Y.; Yang, J. H.; Zhao, B. V_2O_5/vertically-aligned carbon nanotubes as negative electrode for asymmetric supercapacitor in neutral aqueous electrolyte. *J. Colloid Interface Sci.* **2021**, *588*, 847–856.
[44] Chen, L. L.; Huang, Y. C.; Li, H. T.; Gao, R. L.; Tang, H.; Chen, J. W.; Wang, Y. F.; Liao, M. H.; Wu, C. D. Polyoxometalates derived N@Mo_2C/V_2O_3 cluster heterostructure for accelerated alkaline hydrogen evolution reaction. *Polyoxometalates*, in press, DOI:

10.26599/POM.2026.9140110.
[45] Biesinger, M. C.; Lau, L. W. M.; Gerson, A. R.; Smart, R. S. C. Resolving surface chemical states in XPS analysis of first row transition metals, oxides and hydroxides: Sc, Ti, V, Cu and Zn. *Appl. Surf. Sci.* **2010**, *257*, 887–898.
[46] Zheng, S. H.; Chen, J. P.; Wu, T.; Li, R. M.; Zhao, X. L.; Pang, Y. J.; Pan, Z. H. Rational design of Ni-doped V_2O_5@3D Ni core/shell composites for high-voltage and high-rate aqueous zinc ion batteries. *Materials* **2024**, *17*, 215.
[47] Martínez-Hincapié, R.; Wegner, J.; Anwar, M. U.; Raza-Khan, A.; Franzka, S.; Kleszczynski, S.; Čolić, V. The determination of the electrochemically active surface area and its effects on the electrocatalytic properties of structured nickel electrodes produced by additive manufacturing. *Electrochim. Acta* **2024**, *476*, 143663.
[48] Shinagawa, T.; Garcia-Esparza, A. T.; Takanabe, K. Author correction: Insight on Tafel slopes from a microkinetic analysis of aqueous electrocatalysis for energy conversion. *Sci. Rep.* **2020**, *10*, 6899.
[49] Huang, J. H.; Chen, J. T.; Yao, T.; He, J. F.; Jiang, S.; Sun, Z. H.; Liu, Q. H.; Cheng, W. R.; Hu, F. C.; Jiang, Y. et al. CoOOH nanosheets with high mass activity for water oxidation. *Angew. Chem., Int. Ed.* **2015**, *54*, 8722–8727.

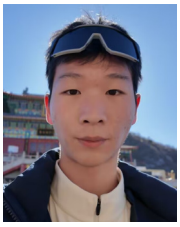

Sizhan Shu is currently a student majoring in Chemical Engineering at Hubei University of Technology, with a research focus on the synthesis and modification of POMs and their applications as precursors in catalysis.

Xiao Feng is currently a student majoring in Chemical Engineering at Hubei University of Technology. His research focuses on the synthesis and modification of POMs, as well as their applications in catalysis. He is dedicated to exploring the performance and mechanisms of POMs-based materials in green organic synthesis and energy conversion.

Jun Sun is currently a student majoring in Chemical Engineering at Hubei University of Technology, with research interests focusing on the catalytic applications of POMs.

Pingfan Wu, distinguished Professor of the inaugural "Nanhu Scholars Program". Director of the Institute of POMs Materials, and Leader of the university-level Premium Course "Organic Chemistry" at Hubei University of Technology, has presided over and completed multiple national, provincial, and ministerial-level research projects, and published more than 50 SCI-indexed papers in international top-tier journals such as *Angew. Chem., Int. Ed.*, *Chem. Eng. J.*, and *J. Mater. Chem. A*. As a pioneer in guiding undergraduates without prior research experience into the field of scientific research, she took the lead in proposing the concept that "undergraduate research training should start upon enrollment", and with university-level innovation and entrepreneurship projects as the incubation carrier, she has successfully practiced the "undergraduate-master-doctoral integrated" talent training model, which has gained widespread recognition in academic circles.